arXiv:hep-ph/9901231v1 6 Jan 1999

CMS NOTE 1998/085

Constraining the minimal supergravity model parameter $\tan\beta$ by measuring the dilepton mass distribution at LHC.

D. Denegri[1], W. Majerotto[2], and L. Rurua[2,3]

[1] *Centre d'Etudes Nucléaire de Saclay, Gif-sur-Yvette, France*

[2] *Institut für Hochenergiephysik, Österreichische Akademie d.Wissenschaften, Vienna, Austria*

[3] *Institute of Physics, Tbilisi, Georgia*

Abstract

We study the dependence on $\tan\beta$ of the event kinematics of final states with $e^+e^-/\mu^+\mu^-/e^\pm\mu^\mp + E_T^{\rm miss} + jets$, as expected in pp collisions at CERN LHC, within the framework of the minimal supergravity model. With increase of $\tan\beta$, the third generation sparticle masses $m_{\tilde{\tau}_1}$ and $m_{\tilde{b}_1}$ decrease due to the increase of the tau and bottom Yukawa couplings. As a result, gluino, stop, sbottom, chargino and neutralino decays to third generation particles and sparticles are enhanced. With $\tan\beta$ rising, we observe a characteristic change in the shape of the dilepton mass spectra in $e^+e^-/\mu^+\mu^- + E_T^{\rm miss} + jets$ versus $e^\pm\mu^\mp + E_T^{\rm miss} + jets$ final states, reflecting the presence of the decays $\tilde{\chi}_2^0 \to \tilde{\ell}_{L,R}^\pm \ell^\mp \to \tilde{\chi}_1^0 \ell^+\ell^-$, $\tilde{\chi}_2^0 \to \tilde{\chi}_1^0 \ell^+\ell^-$ and $\tilde{\chi}_2^0 \to \tilde{\tau}_1^\pm \tau^\mp \to \tilde{\chi}_1^0 \tau^+\tau^-$, $\tilde{\chi}_2^0 \to \tau^+\tau^-\tilde{\chi}_1^0$, respectively. We exploit this effect for constraining the value of $\tan\beta$.

1 Introduction

There is general agreement that new particles predicted by supersymmetry (SUSY) have to be found at LHC, if the appealing conjecture of low energy supersymmetry is correct. Therefore, the discovery potential of LHC for SUSY particles has been studied extensively [1].

Within the last years it became customary to study production and decay of SUSY particles in the context of the 'Minimal Supergravity Model' (mSUGRA) [2]. This model has only five parameters allowing one to study systematically the whole parameter space. The mSUGRA model is based on the minimal supersymmetric extension of the Standard Model (MSSM), which has the minimal possible content with two Higgs doublets (five physical Higgs bosons). The number of parameters of the MSSM is reduced by unification conditions at the GUT point and by making use of the renormalisation group equation (RGE) to calculate the parameters at the electro-weak scale. A further strong constraint of the parameters is given by the requirement of spontaneous electroweak symmetry breaking at this scale (radiative electroweak symmetry breaking). The parameters which remain are: m_0, the common scalar mass at $M_{GUT} = 10^{16}$ GeV, $m_{1/2}$ the unifying gaugino mass, A_0 the common trilinear term at M_{GUT}, $\tan\beta = v_2/v_1$ (with $v_1(v_2)$ being the Higgs vacuum expectation value of the Higgs $H_1^0(H_2^0)$), and $sign(\mu)$, μ being the higgsino mass parameter. This model is incorporated in the Monte Carlo generator ISAJET [3], which is used in our analysis.

A systematic study of all possible signals at LHC as a function of the mSUGRA parameter space was carried out in [4, 5]. In [6] we worked out a method to determine the model parameters m_0 and $m_{1/2}$ with fixed $\tan\beta$ from an analysis of the event kinematics of final states with two same–flavor opposite–sign+ E_T^{miss} +$(jets)$, arising from the decays $\tilde{\chi}_2^0 \to \tilde{\ell}_{L,R}^{\pm}\ell^{\mp} \to \ell^+\ell^-\tilde{\chi}_1^0$, $\tilde{\chi}_2^0 \to \ell^+\ell^-\tilde{\chi}_1^0$, with $\ell = e, \mu$. Both in [4] and in [6] the value of $\tan\beta$ was taken to be ≤ 10. As, however, pointed out in [7, 8, 9] at large $\tan\beta$ ($\tan\beta \gtrsim 10$) the tau and bottom Yukawa coupling $f_{b,\tau} = \frac{gm_{b,\tau}}{\sqrt{2}m_W \cos\beta}$ may become comparable to the electroweak gauge coupling and even to the top Yukawa coupling $f_t = \frac{gm_t}{\sqrt{2}m_W \sin\beta}$. As a consequence, gluino, stop, sbottom, chargino and neutralino decays into third generation particles and sparticles are enhanced when $\tan\beta$ is large [9, 10]. These features make the expected experimental signatures very different from those at low or moderate $\tan\beta$.

Exploiting the fact that decays into τ's are enhanced at large $\tan\beta$, one can get information about the underlying model framework. With this aim, in [9, 10] the reconstruction of τ's by their *hadronic* decays has been considered. In this paper we study the decays $\tilde{\chi}_2^0 \to \tilde{\tau}_1^{\pm}\tau^{\mp} \to \tilde{\chi}_1^0\tau^+\tau^-$ and $\tilde{\chi}_2^0 \to \tilde{\chi}_1^0\tau^+\tau^-$, where the τ's decay *leptonically* leading to final states with two *different*–flavor opposite–sign leptons + E_T^{miss} + jets as a characteristic experimental signature.

In Sec. 2 we discuss the sparticle mass spectrum within mSUGRA. Section 3 is dedicated to a discussion of the production and leptonic decays of $\tilde{\chi}_2^0$ in the mSUGRA parameter space. In Sec. 4 we work out a method to constrain the parameter $\tan\beta$ by analysing the shape of the invariant mass distributions in two same- and different–flavor opposite–sign leptons + E_T^{miss} + jets channels. We summarise our results and give some conclusions in Sec. 5.

2 Sparticle masses in mSUGRA

The masses of the sfermions (squarks and sleptons) of the first two generations are given by the RG equations, [11]:

$$m^2_{\tilde{\ell}_R} = m_0^2 + 0.15 m^2_{1/2} - \sin^2\theta_W D \tag{1}$$

$$m^2_{\tilde{\ell}_L} = m_0^2 + 0.52 m^2_{1/2} - 1/2(1 - 2\sin^2\theta_W) D \tag{2}$$

$$m^2_{\tilde{\nu}} = m_0^2 + 0.52 m^2_{1/2} + 1/2 D \tag{3}$$

$$m^2_{\tilde{u}_R} = m_0^2 + (0.07 + c) m^2_{1/2} + 2/3 \sin^2\theta_W D \tag{4}$$

$$m^2_{\tilde{d}_R} = m_0^2 + (0.02 + c) m^2_{1/2} - 1/3 \sin^2\theta_W D \tag{5}$$

$$m^2_{\tilde{u}_L} = m_0^2 + (0.47 + c) m^2_{1/2} + (1/2 - 2/3 \sin^2\theta_W) D \tag{6}$$

$$m^2_{\tilde{d}_L} = m_0^2 + (0.47 + c) m^2_{1/2} - (1/2 - 1/3 \sin^2\theta_W) D \tag{7}$$

where $D = M_Z^2 \cos 2\beta$ and $4.5 < c < 6$. In the third generation of sfermions $\tilde{f}$ the $\tilde{f}_L - \tilde{f}_R$ mixing may play an important rôle. The mass matrix in the basis $(\tilde{f}_L, \tilde{f}_R)$ with $f = t, b, \tau$ is given by:

$$\mathcal{M}^2_{\tilde{f}} = \begin{pmatrix} m^2_{\tilde{f}_L} & a_f\, m_f \\ a_f\, m_f & m^2_{\tilde{f}_R} \end{pmatrix} \tag{8}$$

with

$$m^2_{\tilde{f}_L} = M^2_{\tilde{Q},\tilde{L}} + m_Z^2 \cos 2\beta (I^f_{3L} - e_f \sin^2\theta_W) + m_f^2 \tag{9}$$

$$m^2_{\tilde{f}_R} = M^2_{\{\tilde{U},\tilde{D},\tilde{R}\}} + m_Z^2 \cos 2\beta e_f \sin^2\theta_W + m_f^2 \tag{10}$$

$$a_f\, m_f = \begin{cases} (A_f - \mu \cot\beta) m_f & \text{for } \tilde{f} = \tilde{t} \\ (A_f - \mu \tan\beta) m_f & \text{for } \tilde{f} = \tilde{b}, \tilde{\tau} \end{cases} \tag{11}$$

where I_3^f is the third component of the weak isospin and e_f the electric charge of the fermion f. $M_{\tilde{Q},\tilde{L},\tilde{U},\tilde{D},\tilde{R}}$ and A_f are soft SUSY-breaking parameters. Note that the mixing term (11) is proportional to the fermion mass and $\cot\beta$ enters in the case of the stop and $\tan\beta$ in that of the sbottom and the stau. Therefore, strong mixing is expected for the stops, but mixing may also be important for sbottom and stau if $\tan\beta$ is large ($\tan\beta \geq 10$) so that one mass eigenstate can be rather light. The mass eigenstates $\tilde{f}_1$ and $\tilde{f}_2$ with masses $m_{\tilde{f}_1}$ and $m_{\tilde{f}_2}$ are obtained by diagonalizing the matrix (8):

$$m^2_{\tilde{f}_1,\tilde{f}_2} = 1/2(m^2_{\tilde{f}_L} + m^2_{\tilde{f}_R}) \mp 1/2\sqrt{(m^2_{\tilde{f}_L} - m^2_{\tilde{f}_R}) + 4 a_f m_f}. \tag{12}$$

In addition, one expects from the RG equations that due to the Yukawa interactions the soft SUSY breaking masses $M_{\tilde{Q},\tilde{L},\tilde{U},\tilde{D},\tilde{R}}$ of the 3rd generation sfermions are smaller than those of the 1st and 2nd generation. As in mSUGRA $|\mu|$ is quite generally large ($|\mu| > M$) the parameter A_f does not play a crucial rôle, especially for large $\tan\beta$ in the case of $\tilde{b}$ and $\tilde{\tau}$. We therefore have taken $A = 0$ in this study.

Within the MSSM the masses of the charginos and neutralinos are determined by the parameters $M = m_{1/2}(M_Z)$, μ, $\tan\beta$ using

$$M_1 \simeq \frac{5}{3}\tan^2\theta_W M \simeq 0.5M, \tag{13}$$

M_1 being the $U(1)$ gaugino mass. In mSUGRA one has quite generally the following mass spectrum:

$$m_{\tilde{\chi}_2^0} \simeq m_{\tilde{\chi}_1^+} \simeq 2m_{\tilde{\chi}_1^0} \simeq M = 0.8m_{1/2},\ m_{\tilde{\chi}_3^0} \simeq m_{\tilde{\chi}_4^0} \simeq |\mu|. \tag{14}$$

In this model $\tilde{\chi}_1^0$ is almost a pure $B-ino$ and $\tilde{\chi}_2^0$ almost a pure W^3-ino. $\tilde{\chi}_1^+$ also has a strong gaugino component. On the other hand, the heavier states $\tilde{\chi}_3^0$, $\tilde{\chi}_4^0$, $\tilde{\chi}_2^\pm$ are higgsino-like. The gluino mass is given by

$$m_{\tilde{g}} = \frac{\alpha_s}{\alpha_2}M \simeq 3M \simeq 2.4m_{1/2} \tag{15}$$

3 Production and leptonic decay of $\tilde{\chi}_2^0$ at large $\tan\beta$

At a hadron collider the neutralinos $\tilde{\chi}_2^0$ are dominantly produced in the decay chain of massive gluinos and squarks, for instance $\tilde{g} \to q\bar{q}\tilde{\chi}_i^0$ or $\tilde{q}_{1,2} \to q\tilde{\chi}_i^0$, $i = 1, 4$, and $\tilde{\chi}_j^0 \to \tilde{\chi}_k^0 Z^0$, $j = 2, 4$, $k = 1, j-1$. These decays have been studied extensively for $\tan\beta \lesssim 10$ in [12]. Squarks and gluino decays for $\tan\beta \gtrsim 10$ have been discussed first in [8]. The collider phenomenology with large $\tan\beta$ has been quite generally discussed in [7, 9], including the chargino and neutralino decays. There are two features which play an important rôle at large $\tan\beta$. First, as shown in section 2 the sbottom $\tilde{b}_1$ and stau $\tilde{\tau}_1$ become lighter. Second, the Yukawa couplings of b and τ $f_{b,\tau} = \frac{g m_{b,\tau}}{\sqrt{2} m_W \cos\beta}$ increase with $\tan\beta$. Both effects lead to a significant enhancement of sbottom and stop production and of decays of gluinos, stops, sbottoms, charginos and neutralinos into third generation particles and sparticles. In particular, the branching ratios of the $\tilde{\chi}_2^0$ to (s)tau's are increasing for large $\tan\beta$ with respect to the corresponding decays into (s)electrons and (s)muons. In Fig. 1 we show the maximum possible branching ratio values (for $m_0 \lesssim 500$ GeV, $m_{1/2} \lesssim 900$ GeV, $\mu < 0$) of the following leptonic decays of $\tilde{\chi}_2^0$, as a function of $\tan\beta$:

$$\tilde{\chi}_2^0 \to \tilde{\chi}_1^0 \ell^+ \ell^-, \tag{16}$$

$$\tilde{\chi}_2^0 \to \tilde{\ell}_L \ell, \tag{17}$$

$$\tilde{\chi}_2^0 \to \tilde{\ell}_R \ell, \tag{18}$$

where $\ell = e$ and μ, and

$$\tilde{\chi}_2^0 \to \tilde{\tau}_1 \tau, \tag{19}$$

$$\tilde{\chi}_2^0 \to \tau^+ \tau^- \tilde{\chi}_1^0. \tag{20}$$

In mSUGRA when $\tilde{\chi}_2^0$ decays into sleptons are kinematically allowed, the sleptons then decay directly into the LSP with $B(\tilde{\ell}_{L,R}^{\pm} \to \tilde{\chi}_1^0 \ell^{\pm}) = 100\%$ and $B(\tilde{\tau}_1 \to \tau \tilde{\chi}_1^0) \sim 100\%$.

As can be seen in Fig. 1, the branching ratio of $\tilde{\chi}_2^0 \to \tilde{\tau}_1 \tau$ can even become 100% for $\tan\beta \geq 10$, if this channel is the only two-body decay channel kinematically allowed. Furthermore, the branching ratio of the three-body decay $\tilde{\chi}_2^0 \to \tilde{\chi}_1^0 \tau^+ \tau^-$ can go up to 90%. It does not reach 100% because there are always competing other three-particle decay channels, in particular $\tilde{\chi}_2^0 \to \tilde{\chi}_1^0 b\bar{b}$. The τ's decay as $\tau^- \to e^- \bar{\nu}_e \nu_\tau, \mu^- \bar{\nu}_\mu \nu_\tau$ with a branching ratio of 17.8% and 17.4%, respectively. Therefore, with $\tan\beta \geq 10$ the decays $\tilde{\chi}_2^0 \to \tilde{\tau}_1 \tau \to \tau^+ \tau^- \tilde{\chi}_1^0$ and $\tilde{\chi}_2^0 \to \tau^+ \tau^- \tilde{\chi}_1^0$ give a contribution to final states with two leptons with opposite charge and the *same flavor*, whereas with $\tan\beta \lesssim 10$ that contribution is negligible compared to that from $\tilde{\chi}_2^0 \to \tilde{\ell}_{L,R}^{\pm} \ell^{\mp} \to \ell^+ \ell^- \tilde{\chi}_1^0$, $\tilde{\chi}_2^0 \to \ell^+ \ell^- \tilde{\chi}_1^0$ with $\ell = e, \mu$. However, the distinctive feature of the $\tilde{\chi}_2^0$ decays into τ's is that they also lead to final states with two opposite sign but *different flavor* leptons.

In Fig. 2 we show for $\tan\beta = 10$, $\mu > 0$ in the $(m_0, m_{1/2})$ plane contour lines for cross-section times branching ratios ($\sigma \times B$) for production of $\tilde{\chi}_2^0$ followed by decays $\tilde{\chi}_2^0 \to \tilde{\ell}_{L,R}^{\pm} \ell^{\mp} \to \ell^+ \ell^- \tilde{\chi}_1^0$, $\tilde{\chi}_2^0 \to \ell^+ \ell^- \tilde{\chi}_1^0$, $\tilde{\chi}_2^0 \to \tilde{\tau}_1^{\pm} \tau^{\mp} \to \tau^+ \tau^- \tilde{\chi}_1^0 \to \ell^+ \nu_\ell \bar{\nu}_\tau \ell^- \bar{\nu}_\ell \nu_\tau \tilde{\chi}_1^0$, $\tilde{\chi}_2^0 \to \tau^+ \tau^- \tilde{\chi}_1^0 \to \ell^+ \nu_\ell \bar{\nu}_\tau \ell^- \bar{\nu}_\ell \nu_\tau \tilde{\chi}_1^0$, with $\ell = e$ and μ. As in the low $\tan\beta$ case we can again define three kinematical domains, determined by the masses of $\tilde{\chi}_2^0$ and the sleptons [6], with the characteristic decays:

domain I ($m_0 \gtrsim 0.6 m_{1/2}, m_{1/2} \lesssim 250$ GeV): $m_{\tilde{\chi}_2^0} \lesssim m_{\tilde{\tau}_1}$, with $\tilde{\chi}_2^0 \to \tilde{\chi}_1^0 \ell\ell$ and $\tilde{\chi}_2^0 \to \tilde{\chi}_1^0 \tau\tau$

domain II ($0.3 m_{1/2} \lesssim m_0 \lesssim 0.6 m_{1/2}$): $m_{\tilde{\ell}_R} < m_{\tilde{\chi}_2^0} < m_{\tilde{\ell}_L}$, with $\tilde{\chi}_2^0 \to \tilde{\ell}_R \ell$ and $\tilde{\chi}_2^0 \to \tilde{\tau}_1 \tau$

domain III ($m_0 \lesssim 0.3 m_{1/2}$): $m_{\tilde{\chi}_2^0} \gtrsim m_{\tilde{\ell}_L}$, with $\tilde{\chi}_2^0 \to \tilde{\ell}_L \ell$

In domains I and II there is an additional source of two opposite–sign lepton final states from decays to tau's and stau's respectively, if $\tan\beta \gtrsim 10$. In domain III the decays $\tilde{\chi}_2^0 \to \tilde{\ell}_R \ell$ and $\tilde{\chi}_2^0 \to \tilde{\tau}_1 \tau$ would be kinematically allowed. As $\tilde{\chi}_2^0$ is almost a W^3-ino these decays are suppressed because $\tilde{\tau}_1 \simeq \tilde{\tau}_R$.

Moreover, comparing to the $\tan\beta = 2$ case [6], one can observe a significant decrease of $\sigma \times B$ values for $\tilde{\chi}_2^0 \to \tilde{\ell}_{L,R} \ell \to \ell^+ \ell^- \tilde{\chi}_1^0$ and $\tilde{\chi}_2^0 \to \ell^+ \ell^- \tilde{\chi}_1^0$ decays. For $\tan\beta \gtrsim 25$ the domain for $\tilde{\chi}_2^0 \to \tilde{\ell}_{L,R} \ell$ almost disappears due to the dominance of the decays $\tilde{\chi}_2^0 \to \tilde{\tau}_1 \tau$, see Fig. 1. This can be seen in Fig. 3 where we show the same as in Fig. 2, but for $\tan\beta = 35$. Here we have only two domains left which are:

domain I ($m_0 \gtrsim m_{1/2}, m_{1/2} \lesssim 250$ GeV): $m_{\tilde{\chi}_2^0} \lesssim m_{\tilde{\tau}_1}$, with $\tilde{\chi}_2^0 \to \tilde{\chi}_1^0 \ell\ell$ and $\tilde{\chi}_2^0 \to \tilde{\chi}_1^0 \tau\tau$

domain II ($0.5 m_{1/2} \lesssim m_0 \lesssim m_{1/2}$): $m_{\tilde{\tau}_1} < m_{\tilde{\chi}_2^0} < m_{\tilde{\ell}_R}$, with $\tilde{\chi}_2^0 \to \tilde{\tau}_1 \tau$

Moreover, as one can see comparing Figs. 2 and 3, the upper theoretically excluded

area is increasing with $\tan\beta$. This is due to the fact that the stau lepton mass becomes lighter than that of $\tilde{\chi}_1^0$ with values of m_0 and $m_{1/2}$ decreasing.

Another interesting feature appearing at large $\tan\beta$ is the enhanced yield of Z^0. This is due to three factors: the larger production cross section for $\tilde{b}_1\tilde{b}_1$ because of the smaller $\tilde{b}_1$ mass, the enhanced branching ratio of $\tilde{b}_1 \to \tilde{\chi}_3^0 b$ due to the Yukawa coupling of b to the Higgsino component of $\tilde{\chi}_3^0$, and to the decay $\tilde{\chi}_3^0 \to Z^0\tilde{\chi}_{1,2}^0$.

Furthermore, in the region $m_{1/2} \gtrsim 250$ GeV, where the decay $\tilde{\chi}_2^0 \to Z^0\tilde{\chi}_1^0$ is kinematically possible, it is generally enhanced compared to low $\tan\beta$, because of the larger Higgsino component of $\tilde{\chi}_2^0$ and $\tilde{\chi}_1^0$ at large $\tan\beta$. There is also a narrow band 260 GeV$\lesssim m_{1/2} \lesssim$ 305 GeV, where the decay $\tilde{\chi}_2^0 \to Z^0\tilde{\chi}_1^0$ is the only two-particle decay kinematically possible because the mass of h^0 is larger at large $\tan\beta$.

4 Constraining $\tan\beta$

4.1 Signatures

At low $\tan\beta$, the decays of $\tilde{\chi}_2^0$ to (s)electrons and (s)muons, Eqs. (16)-(18), dominate over those into (s)tau's, Eqs. (19)-(20), leading to electron and muon pairs in the final states, see Fig. 1. The favored signature to select the decay channels Eqs. (16)-(18) is given by two *same–flavor* opposite-sign leptons $+E_T^{miss}$ + jets final states (SFOS). As is known from previous works [13, 14, 5], the invariant mass distribution of the two leptons has a pronounced edge at the kinematical end–point. With increase of $\tan\beta$ the decays to third generation (s)particles (Eqs. (19)-(20)) are increasing. To select these decays we use the event topology of two *different–flavor* opposite–sign leptons $+E_T^{miss}$ + jets (DFOS).

4.2 Signal and background event simulation

The simulations are done at the particle level with parametrised detector responses based on detailed detector simulations. These parametrisations are adequate for the level of detector properties we want to investigate, and are the only practical ones in view of the multiplicity and complexity of the final state signal and background channels studied. The essential ingredients for the investigation of SUSY channels are the response to jets, $E_T^{\rm miss}$, the lepton identification and isolation capabilities of the detector, and the capability to tag b-jets. The CMS detector simulation program CMSJET 3.2 [16] is used. It contains all significant detector response aspects, calorimeter acceptances and resolutions, granularity, main detector cracks and effects of magnetic field. For more details we refer to Ref. [6, 5].

Standard Model background processes are generated with PYTHIA 5.7 [15]. We use CTEQ2L structure functions. The largest background is due to $t\bar{t}$ production, with both W's decaying into leptons, or one of the leptons from a W decay and the other from the b-decay of the same t-quark. We also considered other Standard Model (SM) backgrounds: $W + jets$, WW, WZ, $Z + jets$, ZZ, $b\bar{b}$ and $\tau\tau$-pair production, with decays into electrons and muons. Chargino pair production $\tilde{\chi}_1^{\pm}\tilde{\chi}_1^{\mp}$ is the largest SUSY background, but gives a small contribution compared to the signal.

4.3 The shape of the dilepton mass distribution in the mSUGRA parameter space

In this section we will analyse the shape of the invariant mass distribution of the two leptons $\ell = e, \mu$, coming from the $\tilde{\chi}_2^0$ decays, Eqs. (16)-(20), considering SFOS and DFOS channels. To this purpose we have investigated the expected dilepton invariant mass distributions for different values of the parameters m_0, $m_{1/2}$, $\tan\beta$, with $\mu > 0$.

In Figs. 4(a)-4(d) we show the invariant mass distributions of the two leptons in the SFOS and DFOS channels at a point $m_0 = 100$ GeV, $m_{1/2} = 190$ GeV, for $\tan\beta =$ 2, 10, 15, 25, respectively ($\mu > 0$). The mass spectrum at this point is: $m_{\tilde{\chi}_2^0} \approx 140$ GeV, $m_{\tilde{\chi}_1^0} \approx 75$ GeV, $m_{\tilde{\ell}_R} \approx 132$ GeV, but $m_{\tilde{\tau}_1}$ decreases from 124 GeV to 91 GeV with the increase of $\tan\beta$.

At this $(m_0, m_{1/2})$ point, which belongs to domain II, the two-step decays $\tilde{\chi}_2^0 \to \tilde{\ell}_R^{\pm}\ell^{\mp} \to \ell^+\ell^-\tilde{\chi}_1^0$ are possible for $\tan\beta \lesssim 25$, but the decays $\tilde{\chi}_2^0 \to \tilde{\tau}_1^{\pm}\tau^{\mp} \to \tau^+\tau^-\tilde{\chi}_1^0$ start to contribute significantly to the final states considered for $\tan\beta \gtrsim 10$. Thus, in Figs. 4(a)-4(d) one can observe a characteristic change of the dilepton mass shape in the SFOS and DFOS channels with increase of $\tan\beta$, reflecting the appearance or disappearance of the corresponding decay modes.

For low $\tan\beta$ ($\lesssim 10$), a pronounced edge is visible in the $M_{\ell^+\ell^-}$ distribution in the SFOS channel with the maximum at [14]:

$$M_{\ell^+\ell^-}^{max} = \frac{\sqrt{(m_{\tilde{\chi}_2^0}^2 - m_{\tilde{\ell}_R}^2)(m_{\tilde{\ell}_R}^2 - m_{\tilde{\chi}_1^0}^2)}}{m_{\tilde{\ell}_R}}, \tag{21}$$

while no characteristic structure in the $M_{\ell^+\ell'^-}$ spectrum is expected in the DFOS case, see Fig. 4(a) for $\tan\beta = 2$. In the DFOS case the difference in magnitude (but not in shape) between the $M_{\ell^+\ell'^-}$ spectrum predicted by the SM and that by mSUGRA is due to internal SUSY background, mainly due to $\tilde{\chi}_1^+\tilde{\chi}_1^-$ pair production from gluino/squark cascade decays.

Fig. 4(b) is as Fig. 4(a), but for $\tan\beta = 10$. In comparison to the $\tan\beta = 2$ case one can see a decrease of the statistics in both the SFOS and DFOS channels for the same integrated luminosity of 5×10^3 pb^{-1}. In both SFOS and DFOS final states, the event rates are by an order of magnitude larger than those according to SM expectations. Moreover, a pronounced deviation in the shape of the $M_{\ell^+\ell'^-}$ spectrum from the expected SM and SUSY background is observable in the low mass region. The corresponding $M_{\tau^+\tau^-}$ spectrum due to the $\tilde{\chi}_2^0$ decays to stau's should have a maximum at:

$$M_{\tau^+\tau^-}^{max} = \frac{\sqrt{(m_{\tilde{\chi}_2^0}^2 - m_{\tilde{\tau}_1}^2)(m_{\tilde{\tau}_1}^2 - m_{\tilde{\chi}_1^0}^2)}}{m_{\tilde{\tau}_1}}. \tag{22}$$

The edge of the ditau spectrum is shifted from $M_{\ell^+\ell^-}^{max} = 37$ GeV to $M_{\tau^+\tau^-}^{max} = 51$ GeV due to the mass difference between $\tilde{\ell}_R$ and $\tilde{\tau}_1$, see Eqs. (21) and (22). But the spectrum of the DFOS channel proceeding through $\tau \to \ell\nu\nu$ decays is not so pronounced as in the SFOS channel having no sharp edge due to the missing momentum taken by four neutrinos from τ decays. Therefore the $\ell^+\ell'^-$ mass is distributed in the lower mass region, below the expected ditau kinematical end point. Thus, a distinctive feature of the $M_{\ell^+\ell'^-}$ spectrum is an enhancement in both shape and magnitude over background in the low mass range ("low–mass enhancement").

A further characteristic difference in the dilepton mass spectrum compared to $\tan\beta = 2$ is the appearance of a Z^0 peak in the SFOS channel, which can clearly be seen in Fig. 4(b). Here the Z^0 peak is due to the decays $\tilde{\chi}_3^0 \to Z^0\tilde{\chi}_2^0$, as explained in Sec. 3.

With further increase of $\tan\beta$, due to the significant increase of $\tilde{\chi}_2^0$ decays into stau's and the corresponding decrease of decays into selectrons and smuons, we observe a deterioration of the sharpness of the edge also in the SFOS channel, see Fig. 4(c) for $\tan\beta = 15$. Another consequence of the change in the relative branching fractions of these decays is that the event rate difference between the SFOS and DFOS channels decreases. This effect is visible by comparing Figs. 4(b) and 4(c). Figure 4(c) also exhibits a decrease of the relative event rate below the two peaks from $\tilde{\chi}_2^0 \to \tilde{\ell}\ell/\tilde{\tau}_1\tau$ and $\tilde{\chi}_3^0 \to Z^0\tilde{\chi}_2^0$ decays.

Finally, at $\tan\beta \simeq 25$, Fig. 4(d), when the decays into stau's are the only decay modes contributing to the final states considered, the dilepton mass spectra in the SFOS and DFOS channels become similar with complete disappearance of sharp edges but a strong low–mass enhancement, and the corresponding event rates become comparable. The low–mass $\ell^+\ell^-$ peak and the Z^0 peak are of the same magnitude.

For comparison of the dilepton mass spectra at this (m_0, $m_{1/2}$) point we used a common set of cuts for all values of $\tan\beta$, requiring two hard isolated leptons with $p_T^{\ell_{1,2}} \geq 10$ GeV in $|\eta| < 2.4$, accompanied by large transverse missing energy, $E_T^{\rm miss} \geq 150$ GeV and jet multiplicity $N_{jet} \geq 3$ with energy $E_T^{jet} \geq 60$ GeV in the rapidity range $|\eta_{jet}| < 4.5$. This point is reachable at low luminosity $\mathcal{L}_{int} = 5 \times 10^3$ pb^{-1} even at the largest $\tan\beta$ shown. The observability of the edges in both the SFOS and DFOS channels is estimated by the criterion $(N_{EV} - N_B)/\sqrt{N_{EV}} \gtrsim 5$ and $(N_{EV} - N_B)/N_B \gtrsim 1.3$, where N_{EV} is the number of events with $M_{\ell^+\ell^{(\prime)-}} \leq M^{max}_{\ell^+\ell^{(\prime)-}}$, and N_B is number of the expected SM and SUSY background events in the same mass range. In case the edge is not very sharp due to the dominance of $\tilde{\chi}_2^0$ decays to stau's, we estimate in practice the kinematical "end-points" $M^{max}_{\ell^+\ell^-}$ and $M^{max}_{\ell^+\ell^{\prime-}}$ by subtracting the event sample with the same kinematics, but containing two same-sign leptons for the DFOS channel, or different-flavor events for the SFOS channel, normalized to the non-threshold region. The precision of the kinematical end-point measurement in this case is estimated to be ± 5 GeV for $M^{max}_{\ell^+\ell^{(\prime)-}} \lesssim 50$ GeV. For $M^{max}_{\ell^+\ell^{(\prime)-}} \gtrsim 50$ GeV the mass difference between $\tilde{\chi}_2^0$ and the sleptons is larger, and the neutrinos can have larger momentum. In this case the technique of reconstructing the kinematical end-point requires a more detailed study and is beyond the scope of this paper.

To illustrate the behaviour of the $M_{\ell^+\ell^-}$ and $M_{\ell^+\ell^{\prime-}}$ spectra at very large $\tan\beta$, we show in Fig. 5 various (m_0, $m_{1/2}$) points with $\tan\beta = 35$. Figure 5(a) clearly exhibits the similarity of the dilepton mass spectra in the SFOS and DFOS channels with comparable event rates, as expected at large $\tan\beta$ from $\tilde{\chi}_2^0$ two–body decays to stau's (domain II). Figures 5(b) represents a (m_0, $m_{1/2}$) point where three-body decays of $\tilde{\chi}_2^0$ are possible. Here the two contributions from the decays Eqs. (16) and (20) are visible in the SFOS channel, while in the DFOS channel only $\tilde{\chi}_2^0$ decays into tau's are selected, see Fig. 5(b). Figure 5(c) shows the $M_{\ell^+\ell^-}$ spectrum at point $m_0 = 800$ GeV, $m_{1/2} = 250$ GeV, $\tan\beta = 35$, $\mu > 0$ with the decays $\tilde{\chi}_2^0 \to \ell^+\ell^-\tilde{\chi}_1^0$, $\ell = e, \mu$. In Figs. 5(a)-5(c) the Z^0 peak is higher than the "low–mass enhancement" as being expected for large $\tan\beta \gtrsim 25$. For $m_{1/2} \gtrsim 450$ GeV, Fig. 5(d), there is only a Z^0 peak left, mainly due to the decays $\tilde{\chi}_3^0 \to Z^0\tilde{\chi}_{1,2}^0$.

To reach the (m_0, $m_{1/2}$) points shown in Fig. 5, a higher luminosity is necessary, $\mathcal{L}_{int} = 5 \times 10^4 - 10^5$ pb^{-1}. Correspondingly harder cuts on the leptons and the missing energy have to be applied: two isolated leptons with $p_T^{\ell_{1,2}} \geq 10-15$ GeV, $E_T^{\rm miss} \geq 200-300$

GeV, $N_{jet} \geq 3$ with $E_T^{jet} \geq 60$ GeV in $|\eta_{jet}| < 4.5$. The parameter region reachable at $\tan\beta = 35$ is limited with $\sigma \times B \sim 0.01$ pb for $\tilde{\chi}_2^0$ decays into stau's and $\sigma \times B \sim 0.1$ pb for $\tilde{\chi}_2^0 \to \ell^+\ell^-\tilde{\chi}_1^0$, see Fig. 3.

5 Summary and Conclusions

In this paper we worked out a method to constrain the parameter $\tan\beta$ of the Minimal Supergravity Model in pp collisions at LHC. The characteristic features arising with increase of $\tan\beta$ are:

1) the $\tilde{\chi}_2^0$ decay branching ratio into (s)taus is increasing, whereas the decay fraction into (s)electrons and (s)muons is decreasing;

2) $\tilde{\chi}_3^0$ production and decays into Z^0 are enhanced.

The method is based on the analysis of the dilepton mass distributions in the simplest experimental signatures, $e^+e^-/\mu^+\mu^- + E_T^{\rm miss} + jets$ and $e^\pm\mu^\mp + E_T^{\rm miss} + jets$. These signatures select different leptonic decays of the neutralinos and hence are sensitive to the value of $\tan\beta$. In particular, events with $e^+e^-/\mu^+\mu^- + E_T^{\rm miss} + jets$ final states mainly contain the decay products from $\tilde{\chi}_2^0$ decays to (s)electrons and (s)muons at low $\tan\beta$ and to leptonically decaying stau's at large $\tan\beta$. Moreover, at large $\tan\beta$, the channel $e^+e^-/\mu^+\mu^- + E_T^{\rm miss} + jets$ allows one to measure the Z^0 boson. At large $\tan\beta$ the topology with $e^\pm\mu^\mp + E_T^{\rm miss} + jets$ selects tau's decaying leptonically.

The dilepton mass distributions from the decays of $\tilde{\chi}_2^0$ to (s)electrons/(s)muons and to (s)tau's have different shapes. The decays to (s)electrons and (s)muons lead to a pronounced edge at the kinematical end point in the $M_{\ell^+\ell^-}$ spectrum, while the edge due to the decays into (s)tau's with tau's decaying into electrons and muons is smeared out because of missing momentum taken away by four neutrinos. The dilepton mass spectrum, however, has a pronounced low–mass enhancement, a peak below the kinematical end point. Therefore, the observation of a "low–mass enhancement" in shape and magnitude in the dilepton mass distribution is regarded as evidence for stau lepton production, particularly so in different flavor final states.

We have made use of the expected characteristic dilepton mass shapes and event rates for identifying the corresponding decays and thus for constraining the value of $\tan\beta$. An important aspect of the method is that no particularly stringent demands on detector performance are required for identifying the tau's from the decays of neutralinos even at high luminosity. Essential is the ability to define and select isolated electrons and muons. Another important aspect of this method is that it may give information on $\tan\beta$ even with low integrated luminosity.

We have shown that:

• An edge in the $M_{\ell^+\ell^-}$ distribution is expected to be visible in the $e^+e^-/\mu^+\mu^- + E_T^{\rm miss} + jets$ channel for $\tan\beta \lesssim 25$ in domain II ($0.3m_{1/2} \lesssim m_0 \lesssim 0.6m_{1/2}$), and for $\tan\beta \lesssim 50$ in domain I ($m_0 \gtrsim 0.6m_{1/2}$, $m_{1/2} \lesssim 250$ GeV). The method to differentiate between two- and three-body decays of $\tilde{\chi}_2^0$ was discussed in Ref. [6];

• In the dilepton mass spectrum a clear deviation in shape and magnitude from the SM and internal SUSY background is expected in $e^\pm\mu^\mp + E_T^{\rm miss} + jets$ final states with $\tan\beta \gtrsim 10$;

• Two components in the dilepton mass spectrum due to three-body $\tilde{\chi}_2^0$ decays to

electrons/muons and to tau's are observed for $\tan\beta \gtrsim 10$.

Combining the results of the analysis of the dilepton mass distributions in $e^+e^-/\mu^+\mu^- + E_T^{\rm miss} + jets$ versus $e^\pm\mu^\mp + E_T^{\rm miss} + jets$ final states, we have found the following criteria for constraining $\tan\beta$ in domain II:

• Observation of an edge in the dilepton mass spectrum in $e^+e^-\&\mu^+\mu^- + E_T^{\rm miss} + jets$ channels, but no deviation from SM and internal SUSY background in that for $e^\pm\mu^\mp + E_T^{\rm miss} + jets$ channel restricts $\tan\beta$ to be $\lesssim 10$;

• Observation of an edge in the dilepton mass spectra in $e^+e^-\&\mu^+\mu^- + E_T^{\rm miss} + jets$ and a low–mass enhancement in $e^\pm\mu^\mp + E_T^{\rm miss} + jets$ channels constrains the value of $\tan\beta$ to $10 \lesssim \tan\beta \lesssim 25$;

• Observation of the similar dilepton mass spectra in $e^+e^-\&\mu^+\mu^- + E_T^{\rm miss} + jets$ and $e^\pm\mu^\mp + E_T^{\rm miss} + jets$ channels with comparable shapes and event rates, indicates $\tan\beta \gtrsim 25$.

A further constraint of $\tan\beta$ can be found by measuring the Z^0 peak in the $e^+e^-\&\mu^+\mu^- + E_T^{\rm miss} + jets$ channel. This channel has the advantage of getting no contribution from SM background what makes the SUSY Z^0 signal event sample very clean. This is especially useful if an edge due to $\tilde{\chi}_2^0$ three-body decays is observed. The absence of a Z^0 peak will restrict $\tan\beta$ to be $\lesssim 2$. We have also analysed the relative event rate in the "low–mass peak" of the $M_{\ell^+\ell^-}$ spectrum and in the Z^0 peak. If both peaks are of the same size the value of $\tan\beta$ should be $\gtrsim 25$.

In the region $10 \lesssim \tan\beta \lesssim 25$, $\tan\beta$ can be determined more precisely by measuring the kinematical end points, $M_{\ell^+\ell^-}^{max}$ in the $e^+e^-\&\mu^+\mu^-$ spectrum and $M_{\ell^+\ell'^-}^{max}$ in the $e^\pm\mu^\mp$ spectrum. Knowing the $M_{\ell^+\ell^-}^{max}$ contour line in the $(m_0, m_{1/2})$ parameter plane [6] with good precision, we can constrain $\tan\beta$ by using the relative event rates $\frac{N_1(e^+e^-\&\mu^+\mu^-)}{N_2(e^\pm\mu^\mp)}$ and $\frac{N_1(e^+e^-\&\mu^+\mu^-)}{N_3(Z^0)}$. Here N_1 is the number of events with $M_{\ell^+\ell^-} \lesssim M_{\ell^+\ell^-}^{max}$, N_2 is the number of events with $M_{\ell^+\ell'^-} \lesssim M_{\ell^+\ell'^-}^{max}$, and N_3 is the number of events in the mass region of Z^0, 86 GeV $< m_{Z^0} <$ 96 GeV. We have found that the $M_{\ell^+\ell^-}^{max}$ contour lines in the $(m_0, m_{1/2})$ parameter plane are almost independent of $\tan\beta$ due to the fact that the masses of $\tilde{\chi}_2^0, \tilde{\chi}_1^0, \tilde{\ell}_R$ do not strongly depend on $\tan\beta$ in mSUGRA.

Quite generally, the observation of a characteristic deviation in the dilepton mass shape from that predicted by the SM background can be considered an evidence for Physics Beyond the Standard Model, in particular SUSY [6].

Acknowledgements

L.R. thanks for financial support by the Austrian Academy of Sciences. This work was also supported by the "Fonds zur Förderung der Wissenschaftlichen Forschung" of Austria, project no. P10843-PHY.

References

[1] H. Baer, X. Tata, and J. Woodside, Phys. Rev. D **45**, 142 (1992);
H. Baer, M. Bisset, X. Tata, and J. Woodside, *ibid.* **46**, 303 (1992);
A. Bartl, W. Majerotto, B. Mösslacher, and N. Oshimo, Z. Phys. C **52**, 477 (1991);
C. Albajar et al., in *Proceedings of the ECFA Large Hadron Collider Workshop*, Aachen, Germany, 1990, ed. by G. Jarlskog and D. Rein, CERN Report No. 90-10, Geneva, Switzerland;
F. Pauss, *ibid.*

H. Baer et al., in *Research Directions for the Decade, Proceedings of the Summer Study*, Snowmass, Colorado, 1990, ed. by E. Berger (World Scientific, Singapore, 1992).

[2] For more recent reviews see, e.g.:
M. Dine, hep–ph/9612389;
F.E. Paige, hep–ph/9801254;
S. Dawson, hep–ph/9712464;
J. Gunion, hep–ph/9801417;
R. Arnowitt and P. Nath, hep–ph/9708254;
S.P. Martin, hep–ph/9709356.

[3] F. Paige and S. Protopopescu, in *Supercollider Physics*, p.41, ed. D. Soper (World Scientific, 1986);
H. Baer, F. Paige, S. Protopopescu, and X. Tata, in *Proceedigns of the Workshop on Physics at Current Accelerators and Supercolliders*, ed. J. Hewett, A. White, and D. Zeppenfeld (Argonne National Laboratory, 1993).

[4] H. Baer, C.-H. Chen, F. Paige, and X. Tata, Phys. Rev. D **52**, 2756 (1995);
I. Hinchliffe, J. Womersley, LBNL–38997;
H. Baer, X. Tata, and J. Woodside , Phys. Rev. D **53**, 6241 (1996);

[5] CMS presentation at the LHCC SUSY Workshop, CERN, Oct. 29–30, 1996, CMS Document 1996–149 (PH-SUSY);
S. Abdullin et al., CMS Note 1998/006, hep-ph/9806366.

[6] D. Denegri, W. Majerotto, L. Rurua, hep-ph/9711357, Phys. Rev. D58, 095010 (1998).

[7] H. Baer, C.-H. Chen, M. Drees, F. Paige, and X. Tata, Phys. Rev. Lett. **79**, 986 (1997).

[8] A. Bartl, W. Majerotto, W. Porod, Z. Phys. C **64**, 499 (1994); err. Z. Phys. C **68**, 518 (1995).

[9] H. Baer, C.-H. Chen, M. Drees, F. Paige, and X. Tata, Phys. Rev. D **58**, 075008 (1998).

[10] H. Baer, C.-H. Chen, M. Drees, F. Paige, and X. Tata, hep-ph/9809223.

[11] K. Inoue, A. Kakuto, H. Komatsu, and S Takeshita, Prog. Theor. Phys. **68**, 927 (1982);
M. Drees and S.P. Martin, hep–ph/9504324.

[12] H. Baer, V. Barger, D. Karatas, and X. Tata, Phys. Rev. D **36**, 96 (1987);
R.M. Barnett, J.F. Gunion, and H.E. Haber, Phys. Rev. Lett. **60**, 401 (1988); Phys. Rev. D **37**, 1892 (1988);
A. Bartl, W. Majerotto, B. Mösslacher, N. Oshimo, and S. Stippel, Phys. Rev. D **43**, 2214 (1991);
A. Bartl, W. Majerotto, and W. Porod, Z. Phys. C **64**, 499 (1994).

[13] H. Baer, K. Hagiwara, X. Tata, Phys. Rev. D **35**, 1598 (1987);
H. Baer, D.D. Karatas, X. Tata, Phys. Rev. D **42**, 2259 (1990) [Fig. 6(a)];
H. Baer, C. Kao, X. Tata, Phys. Rev. D **48**, 5175 (1993);
H. Baer, C.-H. Chen, F. Paige, X. Tata, Phys. Rev. D **50**, 4508 (1994).

[14] F. Paige, Determining SUSY particle masses at LHC, Proc. of the 1996 DPF/DPB Summer Study on High-Energy Physics 'New Directions for High-Energy Physics', Snowmass, Colorado, 1996, p.710;
A. Bartl et al., Supersymmetry at LHC, *ibid.*, p.693;
J. Amundson et al., Report of the Supersymmetry Theory Subgroup, *ibid.*, p.655;
I. Hinchliffe, F.E. Paige, M.D. Shapiro, J. Söderqvist, W. Yao, hep-ph/9610544.

[15] T. Sjöstrand, *Comp. Phys. Com.* **39**, 347 (1986);

T. Sjöstrand and M. Bengtsson, *Comp. Phys. Com.* **43**, 367 (1987);

H.U. Bengtsson and T. Sjöstrand, *Comp. Phys. Com.* **46**, 43 (1987);

T. Sjöstrand, CERN-TH.7112/93.

[16] S. Abdullin, A. Khanov and N. Stepanov, CMS TN/94-180.

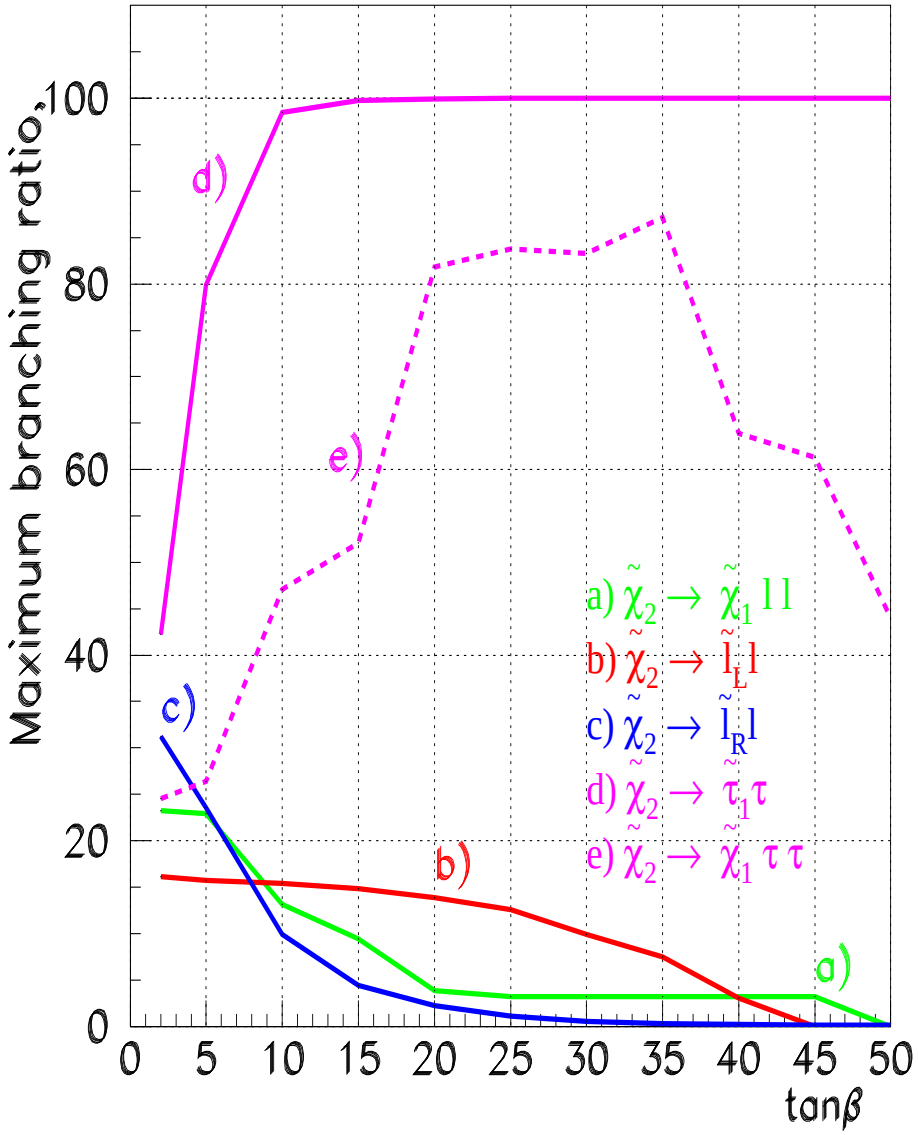

Figure 1: The maximum branching ratio of the decays: a) $\tilde{\chi}_2^0 \to \tilde{\chi}_1^0 \ell^+ \ell^-$, b) $\tilde{\chi}_2^0 \to \tilde{\ell}_L^\pm \ell^\mp$, c) $\tilde{\chi}_2^0 \to \tilde{\ell}_R^\pm \ell^\mp$, d) $\tilde{\chi}_2^0 \to \tilde{\tau}_1^\pm \tau^\mp$, and e) $\tilde{\chi}_2^0 \to \tau^+ \tau^- \tilde{\chi}_1^0$ with $\ell = e$ and μ, for $A_0 = 0$, $\mu > 0$.

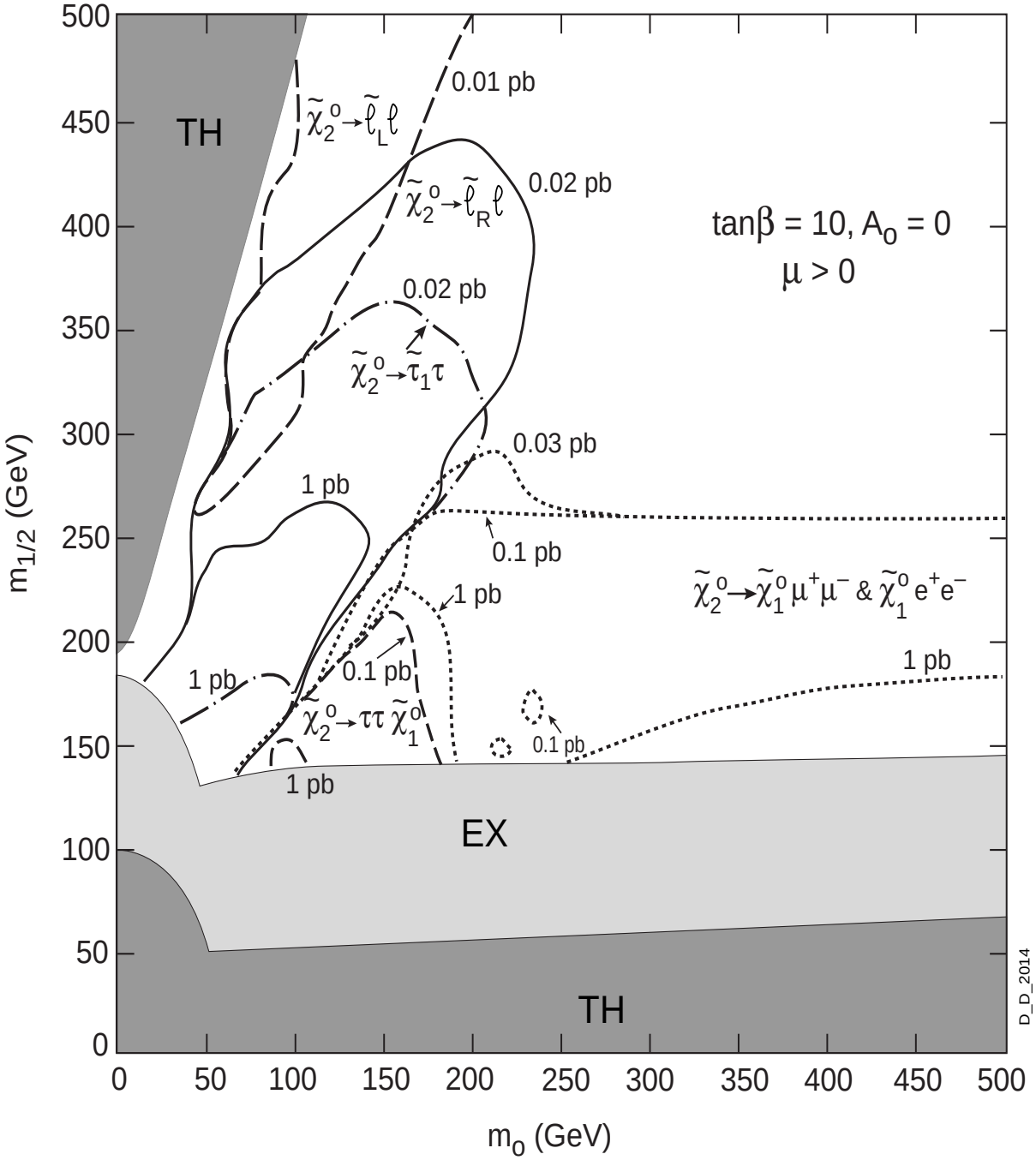

Figure 2: Contour lines for cross-section times branching ratios in the $(m_0, m_{1/2})$ plane for indirect and associated $\tilde{\chi}_2^0$ production followed by decays: $\tilde{\chi}_2^0 \to \tilde{\ell}_R^{\pm}\ell^{\mp} \to \tilde{\chi}_1^0\ell^+\ell^-$ (solid line), $\tilde{\chi}_2^0 \to \tilde{\chi}_1^0\ell^+\ell^-$ (dotted line), $\tilde{\chi}_2^0 \to \tilde{\tau}_1^{\pm}\tau^{\mp} \to \tau^+\tau^-\tilde{\chi}_1^0 \to \ell^+\nu_\ell\bar{\nu}_\tau\,\ell^-\bar{\nu}_\ell\nu_\tau\tilde{\chi}_1^0$ (dashed-dotted line), $\tilde{\chi}_2^0 \to \tau^+\tau^-\tilde{\chi}_1^0 \to \ell^+\nu_\ell\bar{\nu}_\tau\,\ell^-\bar{\nu}_\ell\nu_\tau\tilde{\chi}_1^0$ (short dashed line) $\tilde{\chi}_2^0 \to \tilde{\ell}_L^{\pm}\ell^{\mp} \to \tilde{\chi}_1^0\ell^+\ell^-$ (long dashed line) with $\ell = e$ and μ, for $\tan\beta = 10$, $A_0 = 0$, $\mu > 0$.

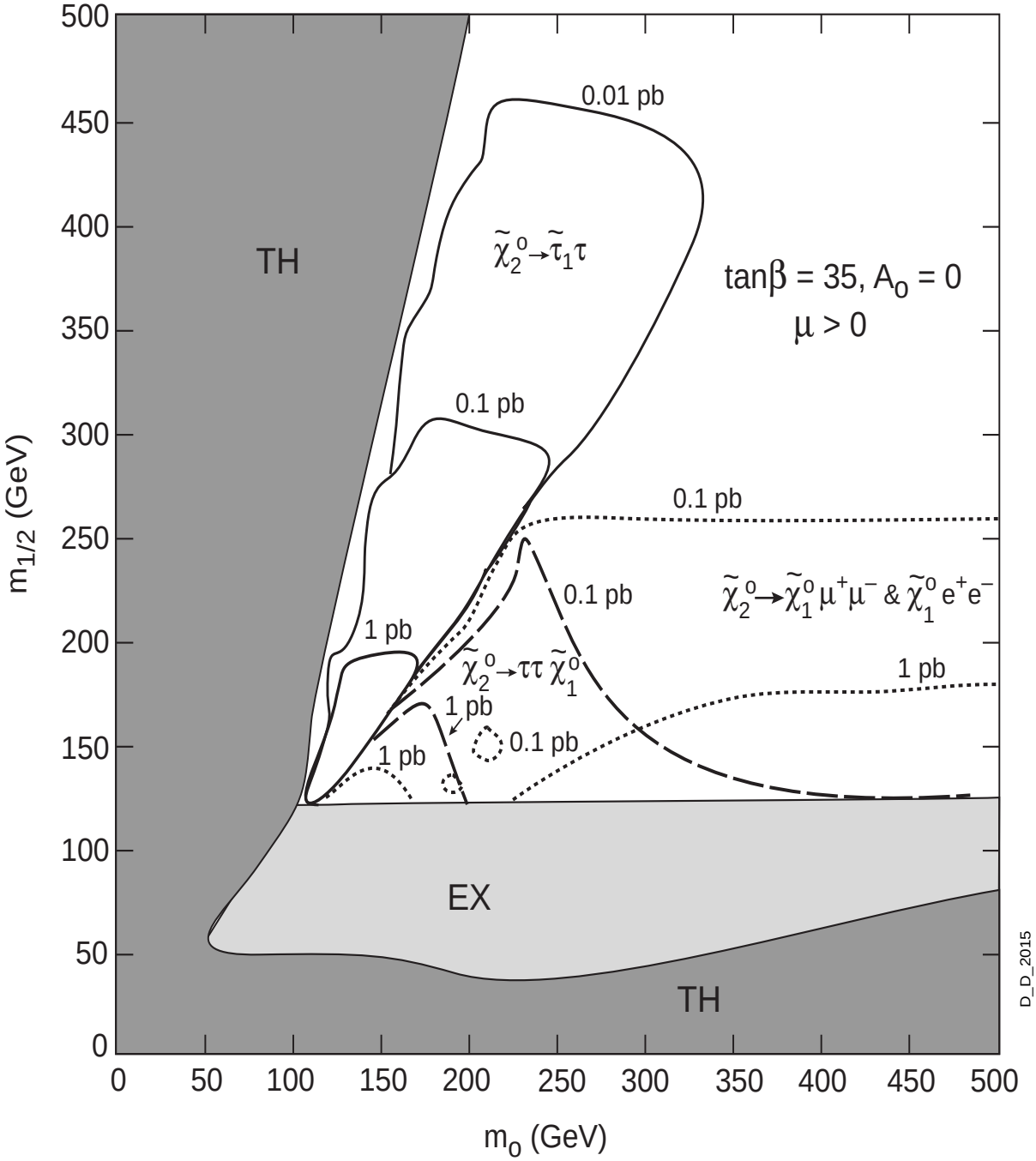

Figure 3: Contour lines for cross-section times branching ratios in the $(m_0, m_{1/2})$ plane for indirect and associated $\tilde{\chi}_2^0$ production followed by decays: $\tilde{\chi}_2^0 \to \tilde{\ell}_R^{\pm}\ell^{\mp} \to \tilde{\chi}_1^0\ell^+\ell^-$ (solid line), $\tilde{\chi}_2^0 \to \tilde{\chi}_1^0\ell^+\ell^-$ (dotted line), $\tilde{\chi}_2^0 \to \tilde{\tau}_1^{\pm}\tau^{\mp} \to \tau^+\tau^-\tilde{\chi}_1^0 \to \ell^+\nu_\ell\bar{\nu}_\tau\,\ell^-\bar{\nu}_\ell\nu_\tau\tilde{\chi}_1^0$ (dashed-dotted line), $\tilde{\chi}_2^0 \to \tau^+\tau^-\tilde{\chi}_1^0 \to \ell^+\nu_\ell\bar{\nu}_\tau\,\ell^-\bar{\nu}_\ell\nu_\tau\tilde{\chi}_1^0$ (short dashed line) $\tilde{\chi}_2^0 \to \tilde{\ell}_L^{\pm}\ell^{\mp} \to \tilde{\chi}_1^0\ell^+\ell^-$ (long dashed line) with $\ell = e$ and μ, for $\tan\beta = 35$, $A_0 = 0$, $\mu > 0$.

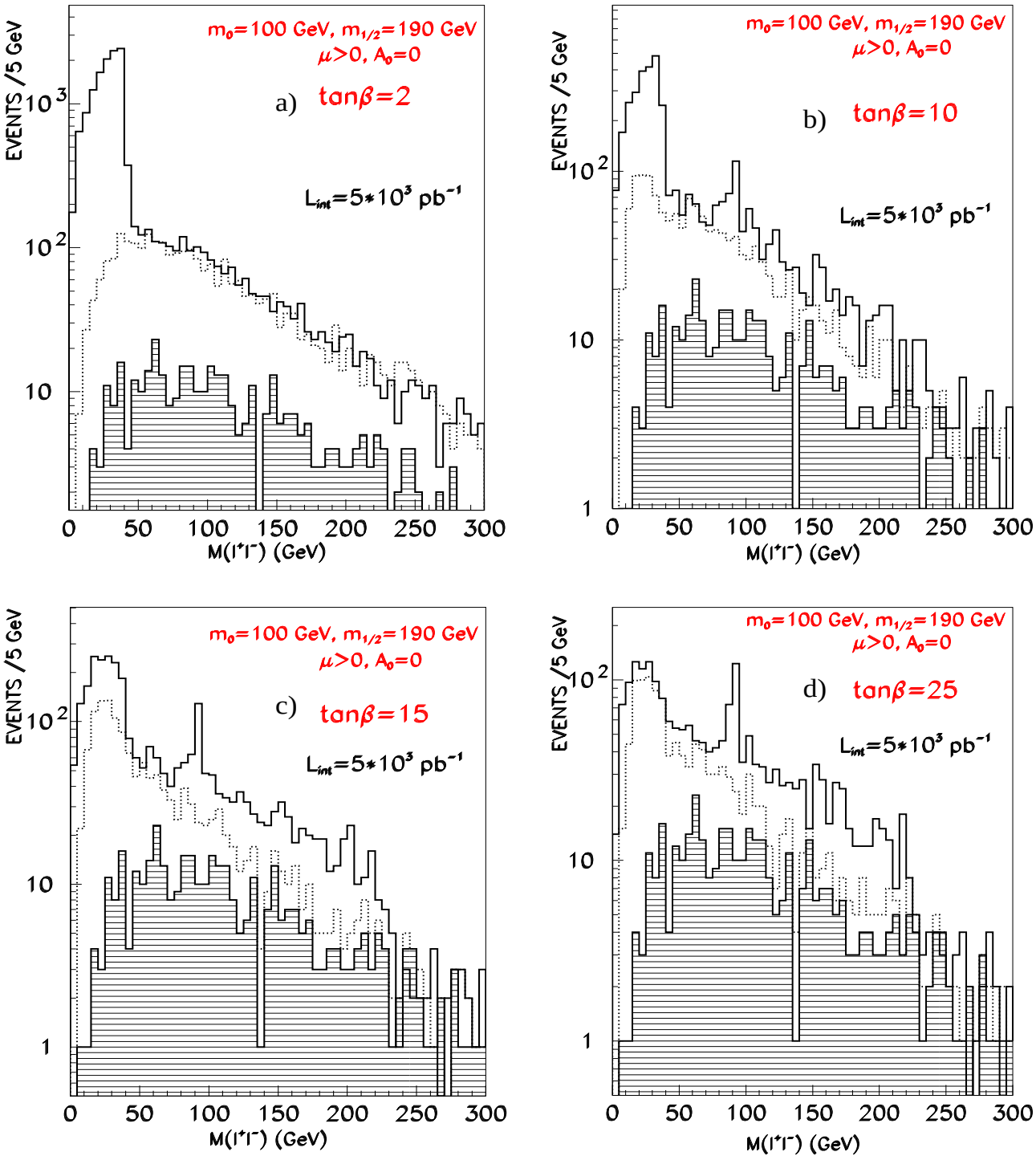

Figure 4: The invariant mass distributions of e^+e^- and $\mu^+\mu^-$ (solid line) and $e^\pm\mu^\mp$ (dotted line) lepton pairs at the point $m_0 = 100$ GeV, $m_{1/2} = 190$ GeV, $\mu > 0$, $A_0 = 0$ with various $\tan\beta = 2, 10, 15, 25$. SM background is also shown (hatched histogram).

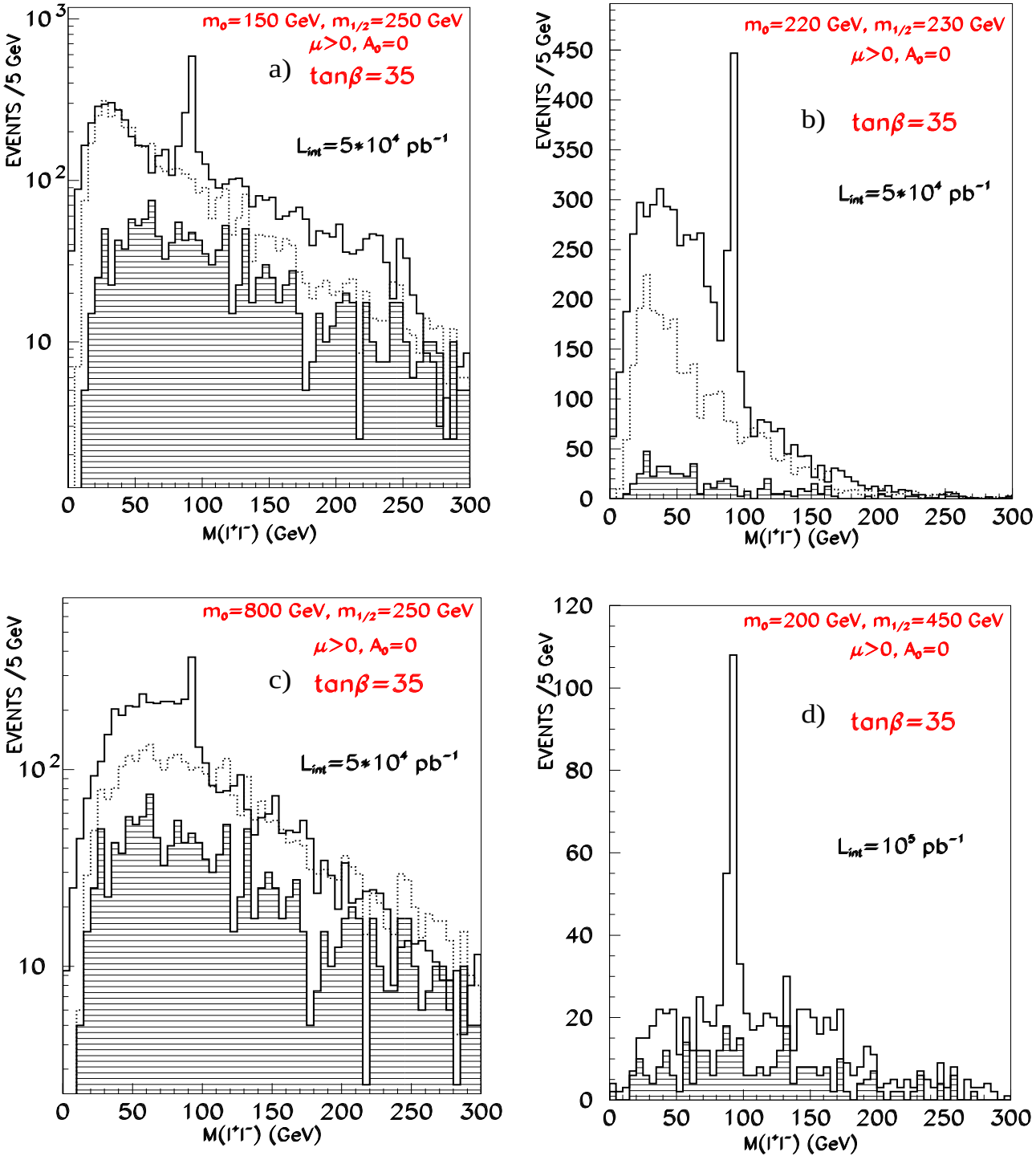

Figure 5: The invariant mass distributions of e^+e^- and $\mu^+\mu^-$ (solid line) and $e^\pm\mu^\mp$ (dotted line) lepton pairs at various $(m_0, m_{1/2})$ points with $\tan\beta = 35$. SM background is also shown (hatched histogram).